Efficient Localization of a Native Metal Ion Within a Protein by Cu(II)-Based EPR Distance Measurements

Journal:	*Physical Chemistry Chemical Physics*
Manuscript ID	CP-ART-11-2018-007143.R1
Article Type:	Paper
Date Submitted by the Author:	14-Jan-2019
Complete List of Authors:	Gamble Jarvi, Austin; University of Pittsburgh, Chemistry Cunningham, Timothy; University of Pittsburgh, Chemistry Saxena, Sunil; University of Pittsburgh, Chemistry

Journal Name

ARTICLE

Efficient Localization of a Native Metal Ion Within a Protein by Cu^{2+}-Based EPR Distance Measurements

Austin Gamble Jarvi,[a] Timothy F. Cunningham [a,b] and Sunil Saxena*[a]

Received 00th January 20xx,
Accepted 00th January 20xx

DOI: 10.1039/x0xx00000x

www.rsc.org/

Electron paramagnetic resonance (EPR) based distance measurements have been exploited to measure protein-protein docking, protein-DNA interactions, substrate binding and metal coordination sites. Here, we use EPR to locate a native paramagnetic metal binding site in a protein with less than 2 Å resolution. We employ a rigid Cu^{2+} binding motif, the double histidine (dHis) motif, in conjunction with double electron electron resonance (DEER) spectroscopy. Specifically, we utilize a multilateration approach to elucidate the native Cu^{2+} binding site in the immunoglobulin binding domain of protein G. Notably, multilateration performed with the dHis motif required only the minimum number of four distance constraints, whereas comparable studies using flexible nitroxide-based spin labels require many more for similar precision. This methodology demonstrates a significant increase in the efficiency of structural determinations via EPR distance measurements uisng the dHis motif.

Introduction

Electron paramagnetic resonance (EPR) spectroscopy in combination with site-directed spin labeling has emerged as a powerful methodology for the determination biomolecular structure.[1] The development of spin labeling techniques has enabled EPR spectroscopy to solve two broad classes of biophysical problems. In the first class, spin labeling is applied to a single biomolecular entity to determine structural features such as solvent accessibility, mobility, and secondary structure.[2] The second class of problems involves spin labeling two or more biomolecular bodies or subunits to determine relative subunit conformation,[3-14] protein-protein interactions,[15-20] protein-nucleic acid interactions,[21-24] substrate binding,[25-28] and metal coordination sites.[29-31]

In order to extract such rich information from doubly spin labeled molecules, pulsed EPR distance measurements are often used.[32-40] The most common of these methodologies, double electron electron resonance (DEER) is capable of accurately determining the distance between two paramagnetic centers in a protein within the range of 2-16 nm.[38, 40-41] Typically, nitroxide based labels are used when performing DEER. These labels are commonly attached to the protein backbone by a flexible tether containing five rotatable bonds.[42] This flexibility introduces significant uncertainty in the interpretation of the EPR distance constraints.[43-44] To overcome this limitation, alternative spin labels, such as Cu^{2+} ions, have been developed.[45-49] Here, we employ a rigid Cu^{2+} labeling technique, the double histidine (dHis) motif, which has been shown to drastically increase the precision of DEER-based distance measurements.[50] Herein, we utilize the dHis motif to determine the location of a native paramagnetic metal binding site within a protein using a multilateration technique. Multilateration methods in three-dimensional space require a minimum of four distance constraints. However, such attempts using nitroxide spin labels have required five-fifteen distance constraints for adequate determination.[26, 28, 30] Similar nitroxide based methodologies using only four constraints have yielded general information regarding ligand binding locations[31] or subunit conformational changes.[13-14] Using the dHis motif, we show that a highly precise determination can be performed using this minimum four distance constraints.

Experimental methods

GB1 mutants were mutated, expressed and purified according to previously published protocols.[50] Samples were prepared in 50 mM NEM buffer at pH 7.4 with 20% v/v glycerol as a cryoprotectant. For EPR experiments 120 µL of protein samples were placed in quartz tubes of I.D. 3 mm, O.D. 4 mm and flash frozen at 80 K for EPR experiments.

All EPR experiments were performed on either a Bruker ElexSys E580 X-band CW/FT Spectrometer with an ER 4118X-MD5 resonator or a Bruker ElexSys E680 X-band CW/FT Spectrometer with an ER 4118X-MD4 resonator. CW experiments were carried out at 80 K with a modulation amplitude of 4 G, a modulation frequency of 100 kHz, a conversion time of 20.48 ms, and a time constant of 10.24 ms. The center field was set at 3100 G with a sweep width of 2000 G over a total of 1024 datapoints. Simulations of the CW spectra were performed with EasySpin.[51]

[a] Department of Chemistry, University of Pittsburgh, Pittsburgh PA 15260, USA.
[b] Present Address: Department of Chemistry, Hanover College, Hanover IN 47243, USA.

Electronic Supplementary Information (ESI) available: Circular dichroism data, raw DEER data, orientational analysis of DEER data, and multilateration confirmation. See DOI: 10.1039/x0xx00000x

The four-pulse DEER experiment[40] was carried out at 20 K using the pulse sequence $(\pi/2)_{\omega A}$–τ– $(\pi)_{\omega A}$–τ+T– $(\pi)_{\omega B}$–τ_2-T– $(\pi)_{\omega A}$–τ_2–echo. A frequency offset of 150 MHz was used between ω_A and ω_B, with ω_A set to the point of highest echo intensity in the Cu^{2+} spectrum, unless otherwise noted. π/2 and π pulses at ω_A were 16 ns and 32 ns respectively. The π pulse at ω_B was 16 ns. The step size was set between 8-16 ns and incremented over 128 points. Raw DEER data was analyzed using DeerAnalysis2016[52]. The distance distributions obtained from DeerAnalysis2016 were then corrected for the proper g-factor.[53]

Circular dichroism was performed using an Olis DSM17 Circular Dichroism Spectrometer. Samples were prepared with 40 µM protein in 20 mM sodium phosphate buffer at pH 7.0. Measurements were performed in 2 mm quartz cells at a temperature of 25 °C from 200 nm to 260 nm with 1 nm increments and a 2 nm bandwidth. Spectra were background corrected with buffer. Melts were collected at 220 nm from 4 °C to 98 °C in 2 °C increments with a 0.5 °C dead band and 2 min equilibration time at each temperature.

Molecular modeling of GB1 and dHis mutants was done using Pymol. Trilateration was performed using MMM[54-55] and mtsslSuite.[56]

Results and discussion

DEER-based multilateration of a native paramagnetic metal binding site was performed on the immunoglobulin binding domain of protein G (GB1). GB1 is a stable globular protein[57] and NMR paramagnetic relaxation enhancement studies have indicated the presence of natively bound Cu^{2+} in GB1.[58] Furthermore, GB1 served as the template on which the dHis motif was developed as a spin labelling method.[50, 59-60] In the original work, the native Cu^{2+} binding was corroborated by EPR data.[50] Additionally, CD data and temperature melts show that the addition of Cu^{2+} to wild type (WT) GB1 does not perturb the protein folding and has a minimal effect on the thermal stability of the protein (Figure S1). These factors make GB1 an excellent system for our applications.

We prepared a series of mutants containing single dHis sites at various locations within GB1. As shown previously, incorporation of the dHis motif does not perturb the folding of GB1.[50, 59-60] Due to the minimum requirement of four constraints for multilateration, four dHis sites were chosen; an α-helical site, 28H/32H, and three β-sheet sites, 6H/8H, 15H/17H, and 42H/44H. These locations distribute the dHis sites across the solvent exposed face of GB1 to provide variety of constraints for multilateration. Figure 1A shows the relative locations of the dHis sites within the crystal structure of WT GB1 (PDB: 2LGI).[61]

We again confirmed the presence of a native Cu^{2+} binding site within the GB1 protein by performing continuous wave (CW) EPR experiments on WT GB1. Figure 1B shows a CW EPR spectrum of WT GB1 in the presence of 10 equivalents of Cu^{2+} (top most spectrum). In these measurements, N-ethylmorpholine (NEM) buffer was used to silence the EPR signal of any Cu^{2+} not bound to the protein.[62] Therefore, the observation of the EPR spectrum seen for WT GB1 in Figure 1B

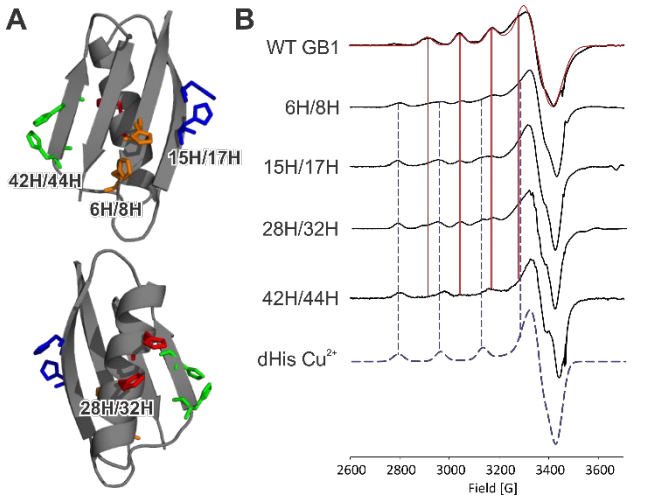

Figure 1. A) The crystal structure of GB1 (PDB: 2LGI)[61] with dHis mutation sites depicted as colored residues. Four sites were chosen, 6H/8H (orange), 15H/17H (blue), 28H/32H (red), and 42H/44H (green). B) CW spectra of WT GB1, four dHis GB1 mutants, and component spectra. All spectra were collected at 80 K in 50 mM NEM buffer at pH 7.4 with 10 eq of Cu^{2+}. The dHis GB1 mutants show two components, one corresponding to the native binding site shown in WT GB1 and the other attributed to dHis-bound Cu^{2+}. The $A_\parallel$ splittings of each component are traced vertically for reference.

can be attributed to Cu^{2+} bound to the protein and confirms the presence of a native binding site. The experimental spectrum was simulated using $g_\parallel = 2.227$, $g_\perp = 2.058$, $A_\parallel = 127$ G, and $A_\perp = 10$ G, and is shown as the red line. These parameters are characteristic of Cu^{2+} in an octahedrally coordination environment.[63]

We performed CW EPR experiments on each double mutant to confirm that each dHis site does not perturb metal binding at the native site. Ten equivalents of Cu^{2+} were added to each mutant to ensure that both the dHis site as well as the native binding site are populated. The CW EPR spectra are shown in Figure 1B. In each sample, two distinct components were observed. The first component corresponded with the $g_\parallel$ and $A_\parallel$ parameters of the WT GB1 signal. These $A_\parallel$ splittings are shown in Figure 1B by the solid red vertical lines that trace the absorbances for each GB1 mutant. The second component is consistent with Cu^{2+} bound to the dHis motif.[50] A simulation of this component is shown as the dashed blue spectrum in Figure 1B. The $A_\parallel$ splittings of this second component are traced vertically through each GB1 spectrum by a dashed blue line. Therefore, the CW EPR results indicate that the dHis mutations do not perturb native binding and that the added Cu^{2+} ions populate both the native binding site as well as the dHis sites.

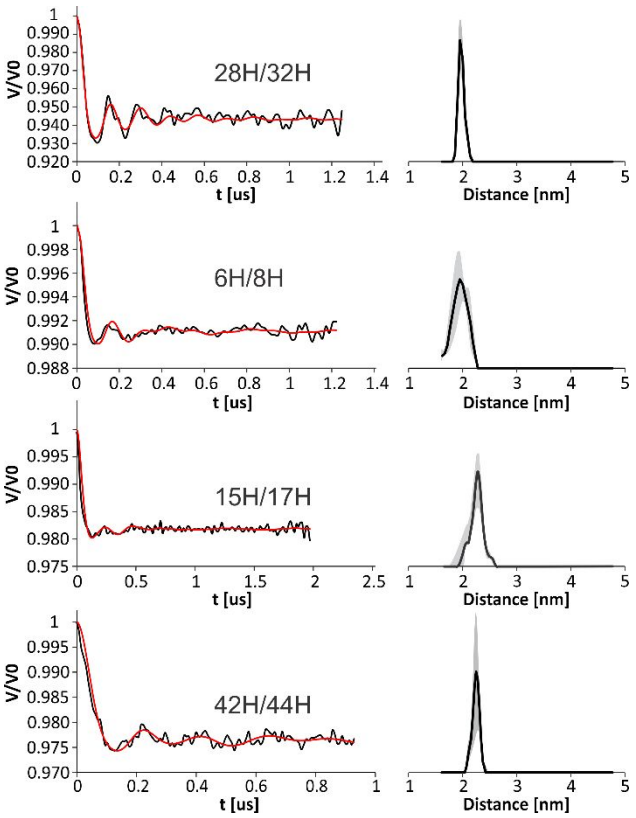

Figure 2. Baseline corrected DEER signal (left) and corresponding distance distributions obtained using Tikhonov regularization (right) for each of the four dHis GB1 mutants. The gray shading on the distance distributions represents the uncertainty of the distance distribution.

We next performed DEER measurements on each dHis double mutant with excess Cu^{2+}. Figure 2 shows the background subtracted time domain DEER signals obtained at $g_{\perp}$ for each mutant and their corresponding distance distributions as determined via Tikhonov regularization (raw data shown in Figure S2). The most probable distances and standard deviations (s.d.) were found to be 1.97±0.05 nm (mean±s.d.) for 28H/32H, 1.96±0.15 nm for 6H/8H, 2.31±0.10 nm for 15H/17H, and 2.25±0.08 nm for 42H/44H. Because of the low affinity of Cu^{2+} for the WT site, poor modulation depths and signals were obtained for DEER at $g_{\parallel}$. 28H/32H GB1 provided a signal to noise ratio adequate for a general analysis, and showed dipolar modulations as well as a resultant distance distribution that agrees with the most probable distance found at $g_{\perp}$ within 0.1 nm (Figure S3). Additionally, past work with Cu^{2+}-based DEER[46] and with rigid dHis motifs in this system[50, 64] and others[65] shows that orientational effects are not typically observed under the experimental conditions used herein. Therefore, we do not expect any orientational effects in this data.

The standard deviations of the distributions are within a range of 0.05-0.15 nm. These standard deviations are notably smaller than those of comparable studies using nitroxide spin labels. For nitroxide-based measurements performed to determine the Cu^{2+} binding center of azurin, standard deviations ranged between 0.1-0.32 nm.[30] Likewise, in using nitroxides to determine the Cu^{2+} binding in EcoRI, DEER distributions reported standard deviations between 0.2-0.3 nm.[29] The standard deviations are system dependent, taking into account

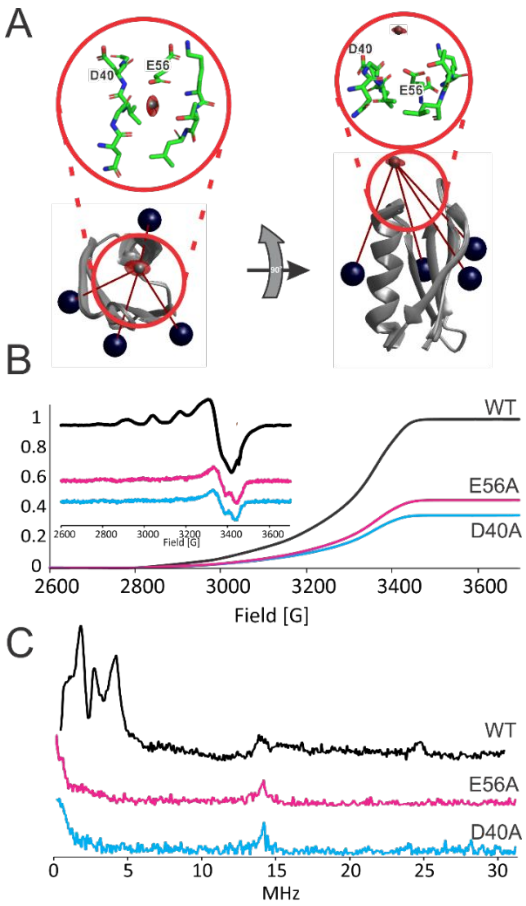

Figure 3. A) Multilateration results using experimental DEER constraints with MMM. The GB1 crystal structure is shown in gray, with the dark blue spheres representing the Cu^{2+} bound to the dHis sites. The circled insets show the local coordination environment of the target of the multilateration. B) Double integrated intensity of WT GB1 (black), E56A GB1 (pink), D40A GB1 (blue) with 10 equivalents Cu^{2+}. The inset shows the first derivative CW EPR spectra. The intensities were normalized to the maximum intensity of the WT sample. C) ESEEM spectra for the series of GB1 samples. All samples were in 50 mM NEM buffer.

the site of mutation, flexibility of the backbone, and the spin label employed. However, as we have shown previously, the dHis motif is capable of greatly decreasing the standard deviation of DEER distance distributions within the same system at equivalent sites compared to a common nitroxide label.[50, 65-66]

The distance distributions derived from DEER were then used as constraints to establish the location of the native metal binding site. This was achieved using the Multiscale Modeling of Macromolecules (MMM).[54] MMM is capable of introducing the dHis Cu^{2+} motif to a given crystal structure *in silico.*[55] Using the WT GB1 crystal structure (PDB: 2LGI), we added the four dHis-bound Cu^{2+} ions in MMM, as shown as dark blue spheres in Figure 3A. The mean distances and standard deviations determined by DEER were input for each corresponding dHis site. With the appropriate constraints, MMM is able to perform a multilateration to locate the native metal binding site by calculating constraint overlap. The results of this multilateration are shown in Figure 3A. The calculated location of the natively bound Cu^{2+} is shown as a red ellipsoid, with the center of this area indicated as a grey sphere. Notably, these results were

validated by performing the multilateration using mtsslTrilaterate[56] as shown in Figure S4. The mtsslTrilaterate results place the native Cu^{2+} in the same vicinity as that found via MMM.

The results of this multilateration are noteworthy, as an unambiguous target location was achieved using only the minimum four distance constraints. The multilateration yielded a target ellipsoid with dimensions approximately 1.4 Å x 1.8 Å x 1 Å. In general, four-fifteen distance constraints have been used to ascertain the general location of a substrate or metal ion in literature.[13-14, 26, 28-31] Although a trilateration on GB1 using nitroxide labels would provide the most direct reference, it is useful to compare this work to multilateration results that report errors. For previous work using nitroxide labels, six measurements were necessary to achieve an error in the measurement of 2.6 Å, and an error of 4.4 Å when using the minimum of four constraints.[30] The precision of our results are more comparable with the location of a lipid within the lipoxygenase active site, which yielded a target ellipsoid of dimensions 1.2 Å x 2.3 Å x 3.0 Å using fifteen distance constraints.[26] Using the rigid dHis motif, we showed improved precision with an approximately fourfold decrease in the number of measurements.

The GB1 crystal structure (PDB: 2LGI) then provides insight into the context of the native binding site. In the circled insets in Figure 3A, we have shown the stick representation of the amino acid residues in the general proximity of the multilateration target. Notably, within this region are the aspartic and glutamic acid residues D40 and E56, respectively. These specific amino acids contain a negatively charged carboxylate group at physiological pH which is known to participate in metal ion coordination in metalloproteins.[67] NMR relaxation enhancement studies on GB1 have indicated D40 as one of the residues involved in native binding sites.[58] Additionally, E56 is the terminal residue of GB1 and thus the carboxylate group of the C-terminus may play a role in the native binding. Based on their proximity to the multilateration target and the corroboration of NMR data, it is likely that these residues are involved in the native Cu^{2+} binding site in GB1.

The involvement of these residues was confirmed performing D40A and E56A mutations. Alanine was chosen as it does not contain groups that coordinate with Cu^{2+}. Cu^{2+} was added to each mutant and CW spectra were collected and doubly integrated in order to compare the amount of bound Cu^{2+} relative to WT GB1 (shown in Figure 3B). These experiments were again performed in NEM buffer to silence free Cu^{2+}. The single mutants E56A and D40A showed reduction of natively bound Cu^{2+} by 55% and 65%, respectively. Circular dichroism (CD) spectra of the alanine mutants are qualitatively similar to that of WT GB1 (Figure S5). Given that the Cu^{2+} binding site involves the C-terminal residue, the remaining presence of Cu^{2+} may be due to a continuing coordination to the C-terminus carboxylate, which will be present regardless of the amino acid residue. Note that C-terminal binding can be removed by the use of a Cu^{2+} chelator such as iminodiacetic acid or nitrilotriacetic acid.[50, 59-60]

Finally, we performed electron spin echo envelope modulation (ESEEM) on WT, D40A, and E56A GB1, as shown in Figure 3C. ESEEM is a pulsed EPR technique that is sensitive to nuclear spins within 3-10 Å of the unpaired electron. The ESEEM spectrum for Cu^{2+} bound to WT GB1 exhibits a signal characteristic of the amide nitrogen of the peptide backbone,[68-69] which is consistent with coordination of Cu^{2+} to the functional group of an amino acid. These features are noticeably absent from the GB1 alanine mutants. This absence indicates that the alanine mutations are in fact perturbing the coordination environment of the Cu^{2+} ions within the protein. The peak around 14 MHz, which is consistent for all samples, is due to surrounding hydrogens. The ESEEM and CW data taken together support the results of our multilateration and the supposition that residues D40 and E56 are involved in the native binding of Cu^{2+}.

Conclusions

In summary, in this work we demonstrate the use of the dHis Cu^{2+} binding motif for the multilateration of a native paramagnetic metal binding site within a protein. Using this rigid spin labelling technique, precise multilateration results were obtained using the minimum number of distance constraints necessary for a three-dimensional system. The calculated multilateration results were confirmed by mutating the residues D40 and E56 to alanines, effectively removing their ability to coordinate Cu^{2+} ions. These mutants showed a significant decrease in Cu^{2+} binding. This work shows a distinct advantage of the dHis Cu^{2+} motif for structural assessment over nitroxide-based spin labels. This methodology is of interest to a wide class of metalloproteins. In these proteins the metal ions can act as agonists to control protein structural and conformational shifts, regulate the catalysis of enzymes, and facilitate their movement throughout a living body via transport proteins. Therefore, the precise determination of the location of these metal binding sites is important for our understanding of the protein's mechanism and function. Such dHis based approaches expand its current purview[64-66] into a class of problems relating to protein-protein docking, protein-nucleic acid interactions, and substrate binding.

Conflicts of interest

There are no conflicts to declare.

Acknowledgements

We thank Prof. Seth Horne (University of Pittsburgh) for his help in the interpretation of circular dichroism results. This data was supported by the National Science Foundation (NSF MCB-1613007). The EPR spectrometer was supported by the National Science Foundation (NSF MRI-1725678).

Notes and references

1. Hubbell, W. L., Altenbach, C., *Cur. Opin. Struct. Biol.* **1994,** *4*, 566-573.
2. Hubbell, W. L., McHaourab, H. S., Altenbach, C., Lietzow, M. A., *Structure* **1996,** *4* (7), 779-783.
3. Altenbach, C., Kusnetzow, A. K., Ernst, O. P., Hofmann, K. P., Hubbell, W. L., *Proc. Natl. Acad. Sci.* **2008,** *105* (21), 7439-7444.
4. Ward, R., Zoltner, M., Beer, L., El Mkami, H., Henderson, I. R., Palmer, T., Norman, D. G., *Structure* **2009,** *17* (9), 1187-1194.
5. Singh, V., Azarkh, M., Exner, T. E., Hartig, J. S., Drescher, M., *Angew. Chem. Int. Ed.* **2009,** *48* (51), 9728-9730.
6. Georgieva, E. R., Borbat, P. P., Ginter, C., Freed, J. H., Boudker, O., *Nat. Struct. Mol. Biol.* **2013,** *20*, 215.
7. Hänelt, I., Wunnicke, D., Bordignon, E., Steinhoff, H.-J., Slotboom, D. J., *Nat. Struct. Mol. Biol.* **2013,** *20*, 210.
8. Dalmas, O., Sompornpisut, P., Bezanilla, F., Perozo, E., *Nat. Commun.* **2014,** *5*, 3590.
9. Liu, Z., Casey, T. M., Blackburn, M. E., Huang, X., Pham, L., de Vera, I. M. S., Carter, J. D., Kear-Scott, J. L., Veloro, A. M., Galiano, L., Fanucci, G. E., *Phys. Chem. Chem. Phys.* **2016,** *18* (8), 5819-5831.
10. Grytz, C. M., Marko, A., Cekan, P., Sigurdsson, S. T., Prisner, T. F., *Phys. Chem. Chem. Phys.* **2016,** *18*, 2993-3002.
11. Verhalen, B., Dastvan, R., Thangapandian, S., Peskova, Y., Koteiche, H. A., Nakamoto, R. K., Tajkhorshid, E., McHaourab, H. S., *Nature* **2017,** *543*, 738.
12. Assafa, T. E., Anders, K., Linne, U., Essen, L.-O., Bordignon, E., *Structure* **2018,** *26* (11), 1534-1545.e4.
13. Piotr, G. F., *Journal of Physics: Condensed Matter* **2005,** *17* (18), S1459.
14. López, C. J., Yang, Z., Altenbach, C., Hubbell, W. L., *Proceedings of the National Academy of Sciences of the United States of America* **2013,** *110* (46), E4306-E4315.
15. Park, S.-Y., Borbat, P. P., Gonzalez-Bonet, G., Bhatnagar, J., Pollard, A. M., Freed, J. H., Bilwes, A. M., Crane, B. R., *Nat. Struct. Mol. Biol.* **2006,** *13* (5), 400-407.
16. Hanson, S. M., Dawson, E. S., Francis, D. J., Van Eps, N., Klug, C. S., Hubbell, W. L., Meiler, J., Gurevich, V. V., *Structure* **2008,** *16* (6), 924-934.
17. DeBerg, Hannah A., Bankston, John R., Rosenbaum, Joel C., Brzovic, Peter S., Zagotta, William N., Stoll, S., *Structure* **2015,** *23* (4), 734-744.
18. Valera, S., Ackermann, K., Pliotas, C., Huang, H., Naismith, J. H., Bode, B. E., *Chemistry – A European Journal* **2016,** *22* (14), 4700-4703.
19. Dawidowski, D., Cafiso, David S., *Structure* **2016,** *24* (3), 392-400.
20. Milikisiyants, S., Wang, S., Munro, R. A., Donohue, M., Ward, M. E., Bolton, D., Brown, L. S., Smirnova, T. I., Ladizhansky, V., Smirnov, A. I., *Journal of molecular biology* **2017,** *429* (12), 1903-1920.
21. Stone, K. M., Townsend, J. E., Sarver, J., Sapienza, P. J., Saxena, S., Jen-Jacobson, L., *Angew. Chem. Int. Ed.* **2008,** *47*, 10192-10194.
22. Ruthstein, S., Ji, M., Mehta, P., Jen-Jacobson, L., Saxena, S., *J. Phys. Chem. B.* **2013,** *117*, 6227-6230.
23. Duss, O., Yulikov, M., Jeschke, G., Allain, F. H., *Nat. Commun.* **2014,** *5*, 3669.
24. Sameach, H., Narunsky, A., Azoulay-Ginsburg, S., Gevorkyan-Aiapetov, L., Zehavi, Y., Moskovitz, Y., Juven-Gershon, T., Ben-Tal, N., Ruthstein, S., *Structure* **2017,** *25* (7), 988-996.
25. Upadhyay, A. K., Borbat, P. P., Wang, J., Freed, J. H., Edmondson, D. E., *Biochemistry* **2008,** *47* (6), 1554-1566.
26. Gaffney, Betty J., Bradshaw, Miles D., Frausto, Stephen D., Wu, F., Freed, Jack H., Borbat, P., *Biophys. J.* **2012,** *103* (10), 2134-2144.
27. Yin, D. M., Hannam, J. S., Schmitz, A., Schiemann, O., Hagelueken, G., Famulok, M., *Angew. Chem. Int. Ed.* **2017,** *56* (29), 8417-8421.
28. Steed, P. R., Stein, R. A., Mishra, S., Goodman, M. C., McHaourab, H. S., *Biochemistry* **2013,** *52* (34), 5790-5799.
29. Yang, Z., Kurpiewski, M. R., Ji, M., Townsend, J. E., Mehta, P., Jen-Jacobson, L., Saxena, S., *Proc. Natl. Acad. Sci. USA* **2012,** *109* (17), E993-1000.
30. Abdullin, D., Florin, N., Hagelueken, G., Schiemann, O., *Angew. Chem. Int. Ed.* **2015,** *54* (6), 1827-1831.
31. Evans, Eric G. B., Pushie, M. J., Markham, Kate A., Lee, H.-W., Millhauser, Glenn L., *Structure* **2016,** *24* (7), 1057-1067.
32. Saxena, S., Freed, J. H., *Chemical Physics Letters* **1996,** *251* (1–2), 102-110.
33. Borbat, P. P., Freed, J. H., *Chemical Physics Letters* **1999,** *313*, 145-154.
34. Bonora, M., Becker, J., Saxena, S., *Journal of Magnetic Resonance* **2004,** *170* (2), 278-83.
35. Becker, J. S., Saxena, S., *Chemical Physics Letters* **2005,** *414*, 248-252.
36. Kulik, L. V., Dzuba, S. A., Grigoryev, I. A., Tsvetkov, Y. D., *Chemical Physics Letters* **2001,** *343* (3), 315-324.
37. Milikisyants, S., Scarpelli, F., Finiguerra, M. G., Ubbink, M., Huber, M., *Journal of Magnetic Resonance* **2009,** *201* (1), 48-56.
38. Milov, A., Maryasov, A., Tsvetkov, Y. D., *Applied Magnetic Resonance* **1998,** *15* (1), 107-143.
39. Jeschke, G., Pannier, M., Godt, A., Spiess, H. W., *Chemical Physics Letters* **2000,** *331* (2), 243-252.
40. Pannier, M., Veit, S., Godt, A., Jeschke, G., Spiess, H. W., *J. Magn. Res.* **2000,** *142*, 331-340.
41. Schmidt, T., Wälti, M. A., Baber, J. L., Hustedt, E. J., Clore, G. M., *Angew. Chem. Int. Ed.* **2016,** *128* (51), 16137-16141.
42. Tombolato, F., Ferrarini, A., Freed, J. H., *J. Phys. Chem. B* **2006,** *110*, 26248-26259.
43. Sarver, J. L., Townsend, J. E., Rajapakse, G., Jen-Jacobson, L., Saxena, S., *J. Phys. Chem. B.* **2012,** *116*, 4024.
44. Fajer, P., Fajer, M., Zawrotny, M., Yang, W., Chapter Twenty-Three - Full Atom Simulations of Spin Label Conformations. In *Methods in Enzymology*, Qin, P. Z.; Warncke, K., Eds. Academic Press: 2015; Vol. 563, pp 623-642.
45. Yang, Z., Becker, J., Saxena, S., *J. Magn. Reson.* **2007,** *188*, 337-343.
46. Yang, Z., Kise, D., Saxena, S., *J. Phys. Chem. B* **2010,** *114* (18), 6165-6174.
47. Yang, Z., Ji, M., Saxena, S., *Appl. Magn. Reson.* **2010,** *39* (4), 487-500.
48. Cunningham, T. F., Shannon, M. D., Putterman, M. R., Arachchige, R. J., Sengupta, I., Gao, M., Jaroniec, C. P., Saxena, S., *J. Phys. Chem. B* **2015,** *119*, 2839-2843.
49. Merz, G. E., Borbat, P. P., Muok, A. R., Srivastava, M.,

Bunck, D. N., Freed, J. H., Crane, B. R., *J. Phys. Chem. B* **2018**.
50. Cunningham, T. F., Putterman, M. R., Desai, A., Horne, W. S., Saxena, S., *Angew. Chem. Intl. Ed.* **2015,** *54*, 6330.
51. Stoll, S., Schweiger, A., *J. Magn. Res.* **2006,** *178* (1), 42-55.
52. Jeschke, G., Chechik, V., Ionita, P., Godt, A., Zimmermann, H., Banham, J., Timmel, C., Hilger, D., Jung, H., *Appl. Magn. Reson.* **2006,** *30*, 473-498.
53. Bowen, A. M., Jones, M. W., Lovett, J. E., Gaule, T. G., McPherson, M. J., Dilworth, J. R., Timmel, C. R., Harmer, J. R., *Phys. Chem. Chem. Phys.* **2016,** *18* (8), 5981-5994.
54. Jeschke, G., *Protein Sci.* **2018,** *27* (1), 76-85.
55. Ghosh, S., Saxena, S., Jeschke, G., *Appl. Magn. Reson.* **2018,** *49* (11), 1281-1298.
56. Hagelueken, G., Abdullin, D., Ward, R., Schiemann, O., *Mol. Phys.* **2013,** *111* (18-19), 2757-2766.
57. Gronenborn, A. M., Filpula, D. R., Essig, N. Z., Achari, A., Whitlow, M., Wingfield, P. T., Clore, G. M., *Science* **1991,** *253*, 657-661.
58. Nadaud, P. S., Sengupta, I., Helmus, J. J., Jaroniec, C. P., *J. Biol. NMR* **2011,** *51* (3), 293.
59. Lawless, M. J., Ghosh, S., Cunningham, T. F., Shimshi, A., Saxena, S., *Phys. Chem. Chem. Phys.* **2017,** *19*, 20959-20967.
60. Ghosh, S., Lawless, M. J., Rule, G. S., Saxena, S., *J. Magn. Reson.* **2018,** *286*, 163-171.
61. Wylie, B. J., Sperling, L. J., Nieuwkoop, A. J., Franks, W. T., Oldfield, E., Rienstra, C. M., *Proc. Natl. Acad. Sci. USA* **2011,** *108*, 16974-16979.
62. Syme, C. D., Nadal, R. C., Rigby, S. E. J., Viles, J. H., *J. Biol. Chem.* **2004,** *279*, 18169-18177.
63. Peisach, J., Blumberg, W. E., *Arch. Biochem. Biophys.* **1974,** *195*, 691-708.
64. Gamble Jarvi, A., Ranguelova, K., Ghosh, S., Weber, R. T., Saxena, S., *J. Phys. Chem. B* **2018,** *DOI: 10.1021/acs.jpcb.8b07727*.
65. Lawless, M. J., Pettersson, J. R., Rule, G. S., Lanni, F., Saxena, S., *Biophys. J.* **2018,** *114* (3), 592-601.
66. Sameach, H., Ghosh, S., Gevorkyan-Airapetov, L., Saxena, S., Ruthstein, S., *Angewandte Chemie International Edition* (doi:10.1002/anie.201810656).
67. Tainer, J. A., Roberts, V. A., Getzoff, E. D., *Curr. Opin. Biotechnol.* **1991,** *2* (4), 582-591.
68. McCracken, J., Vassiliev, I. R., Yang, E.-C., Range, K., Barry, B. A., *J. Phys. Chem. B* **2007,** *111* (23), 6586-6592.
69. Cammack, R., Chapman, A., McCracken, J., Cornelius, J. B., Peisach, J., Weiner, J. H., *Biochim. Biophys. Acta, Protein Struct. Mol. Enzymol.* **1988,** *956* (3), 307-312.

Efficient Localization of a Native Metal Ion Within a Protein by Cu^{2+}-Based EPR Distance Measurements

Austin Gamble Jarvi, Timothy F. Cunningham, and Sunil Saxena

A native paramagnetic metal binding site in a protein is located with less than 2 Å resolution by a combination of double histidine (dHis) based Cu^{2+} labeling and long range distance measurements by EPR.